

Fabrication mechanism of nanostructured HA/TNTs biomedical coatings: an improvement in nanomechanical and in vitro biological responses

Shahab Ahmadi¹ · Zohreh Riahi¹ · Aylar Eslami¹ · S.K. Sadrnezhaad¹

Received: 23 May 2016 / Accepted: 20 July 2016
© Springer Science+Business Media New York 2016

Abstract In this paper, a mechanism for fabrication of nanostructured hydroxyapatite coating on TiO₂ nanotubes is presented. Also, the physical, biological, and nanomechanical properties of the anodized Ti6Al4V alloy consisting TiO₂ nanotubes, electrodeposited hydroxyapatite, and the hydroxyapatite/TiO₂ nanotubes double layer coating on Ti6Al4V alloy implants are compared. Mean cell viability of the samples being 84.63 % for uncoated plate, 91.53 % for electrodeposited hydroxyapatite, and 94.98 % for hydroxyapatite/TiO₂ nanotubes coated sample were in the acceptable range. Merely anodized prototype had the highest biocompatibility of 110 % with respect to the control sample. Bonding strength of hydroxyapatite deposit to the substrate increased from 12 ± 2 MPa to 25.4 ± 2 MPa using intermediate TiO₂ nanotubes layer. Hardness and elastic modulus of the anodized surface were 956 MPa and 64.7 GPa, respectively. The corresponding values for hydroxyapatite deposit were approximately measured 44.3 MPa and 0.66 GPa, respectively, while the average obtained values for hardness (159.3 MPa) and elastic modulus (2.25 GPa) of the hydroxyapatite/TiO₂ nanotubes double coating improved more than 30 % of the pure hydroxyapatite deposit. Friction coefficient (ξ) of the anodized surface was 0.32 ± 0.02 . The calculated friction coefficient enhanced from 0.65 ± 0.04 for sole hydroxyapatite layer to the 0.46 ± 0.02 for hydroxyapatite/TiO₂ nanotubes due to presence of nanotubular TiO₂ intermediate layer.

1 Introduction

Much attentions are nowadays focused on titanium alloys for hard tissue utilization. Suitable mechanical properties like tensile strength and Young's modulus as well as corrosion resistance and super biocompatibility have been given considerable attention [1–3]. These are not sole requirements of orthopedic and dental implants which interact with the live bone at least at initial stages of the implantation [4, 5]. An example is the encapsulation of the implanted material by fibrous tissue which results in isolation of the implant from surrounding bone and patient suffering of precocious loosening. Surface modification of Ti-based implants needs, therefore, critical consideration [6, 7].

Oh et al. [8] have indicated significant improvements in formation of interlocked cell structure due to TiO₂ nanotubes (TNTs) formation. Das et al. [9] have showed that anodized TNTs are more osteoconductive than untreated alloy. Popat et al. [10] have conducted successful in vivo biocompatibility tests of TNTs. They have observed no adverse immune response through in vivo environment. Hydroxyapatite (HA) can also be used in line with biomedical purposes. The HA coatings have similar composition to bone tissues and thereby, act as a bridge at the interval of bone and implant [11, 12]. The HA coatings can be obtained through different methods including plasma spraying, sol-gel, biomimetic deposition, and electrochemical deposition [13]. Among these methods, electro-deposition is a useful process for getting coatings with controllable thicknesses and complex shapes [14]. Previous studies have indicated that nanostructured surfaces exhibit good biocompatibility and enhanced osteoblast adhesion.

One of the most important characteristics of a hard tissue replacement is the nanomechanical responses at the interface of implant/bone. This property should be more

✉ Shahab Ahmadi
ahmadi.sh67@yahoo.com
sh_ahmadi@mehr.sharif.ir

¹ Advanced Bionanomaterials Laboratory, Department of Materials science and Engineering, Sharif University of Technology, P.O. Box 11365-9466, Tehran, Iran

considered when the biomaterial is implanted at the locations such as knee, shoulder, elbow, and dental implants during implantation which are under more mechanical forces. The introduced torsion, bending, tensile, and shear tensions to the implant could damage the surface layer of implant as result in separation of coating or toxic ion release and finally failure the implanted biomaterial. Short-term stabilization, implant infection, and other adverse consequences could be attributed to the weak surface nanomechanical properties of the coated biomaterials. Accordingly, improving the nanomechanical properties of surface coatings needs critical consideration. Ahmadi et al. [15] have coated different HA/TiO₂ configurations (consisting of pure HA, TNTs layer, HA/TiO₂ nanocomposite, and HA/TNTs double layer coatings) on Ti6Al4V substrate and then adherence of these coatings have been measured. They realized that oriented nanotube layer as an intermediate layer increases the adhesion of the HA deposit to the implant to a maximum value in comparison with other samples.

Although many investigations have done in order to surface modification of metallic implants, no comprehensive study have done on improvement of the mechanical properties of HA-based coatings deposited on Ti6Al4V alloy implants considering with proper biological properties. Accordingly, the aim of this research is to offer a low cost coating method with the best biocompatibility, cell adhesion, proliferation, mineralization, and bone regeneration accompanying with nanomechanical responses of bioactive coating at the interface of implant/bone. To achieve this purpose, TNTs are firstly synthesized. Subsequently, HA is deposited onto the TNTs by means of pulse electrodeposition method. Then, in order to characterize the surfaces and determine the bioactivity and osteogenic cell responses of the coatings, surface analysis techniques, MTT, and alizarin red staining tests are carried out in this research. Finally, adhesion strength, nanoindentation, and nanoscratch tests are applied to study the nanomechanical properties.

2 Experimental procedure

All specimens were mechanically polished by SiC grinding paper and suspensions of 0.3 and 0.05 % Al₂O₃ nanoparticles. The mirror-like samples were cleaned by sonication in acetone at 60 °C for 10 min and then rinsed in deionized water. They were dried with stream of air and then the electrochemical deposition was performed.

2.1 Formation of nanotubes oxide layer

The electrolyte for anodic oxidation contained 1M (NH₄)₂SO₄ solution having 0.5 wt% NH₄F. The electrochemical setup consisted of a conventional two-electrode

configuration having graphite cathode and Ti6Al4V sheet anode. The electrochemical treatment consisted of a potential ramp from the open circuit potential (OCP) to 25 V with sweep rate of 25 mV/s followed by holding of the applied potential at end-potential for 3600 s. The applied potential in anodizing tests has been illustrated in Fig. 1. All anodizing experiments were carried out at room temperature. Finally the anodized implants were dried in a stream of air.

2.2 Pulse electrodeposition of calcium phosphate coating

For electrochemical coating, both anodized and untreated Ti6Al4V alloy samples were used as cathode and a graphite plate as working electrode. The electrodes were immersed in the electrolyte which contained 0.042 M Ca(NO₃)₂, 0.025 M (NH₄)₂HPO₄, 0.1 M NaNO₃ and 2000 ppm H₂O₂. Addition of NaNO₃ was for improvement of the ionic strength of the electrolyte and H₂O₂ for suppression of the evolution of H₂ and promotion of the deposition of the layer. The pH of the electrolyte was adjusted at 5.5 by sodium hydroxide (NaOH) and nitric acid (HNO₃) at 60 °C. Total procedure time was 60 min, and deposition process was done using a potentiostat/galvanostat pulsing current produced by a pulse rectifier as illustrated in Fig. 2. In order to obtain uniform and adherent coatings, electrodeposition was done under the following conditions: Time deposition $t_{\text{on}} = 2$ s with a current density of $J_{\text{on}} = 1$ mA/cm² followed by a breakdown time of $t_{\text{off}} = 5$ s ($J_{\text{off}} = 0$ mA/cm²). All produced samples were dried slowly at 120 °C for 2 h and heated up to 480 °C at the rate of 3 °C/min and held at 480 °C for 2 h. Heat treatment was accomplished to increase the crystallization degree of the calcium phosphate and for phase transformation of TiO₂ layer from amorphous to anatase phase [16–18].

2.3 Morphology and phase structure characterizations

Morphologies of the surface coatings were inspected by high vacuum FE-SEM model SIGMA/VP ZEISS. Before FE-SEM observation, Au was sputtered on the surface of the specimens. Crystal structures of the samples were analyzed by x-ray diffraction (XRD) (X'Pert Pro MPD, PANalytical) using Cu K α radiation of $\lambda = 1.5418$ Å, 2θ angle of 20–90°, scanning rate of 0.02° s⁻¹, time steps of 20 s and X'Pert Highscore plus software data analysis system.

2.4 Biocompatibility in vitro tests

2.4.1 Cell culture

MG-63 osteoblast, human osteosarcoma cell line, were cultured in Dulbecco's Modified Eagles Medium (DMEM,

Fig. 1 Applied potential steps (●) and measured current (■) vs. anodizing time. Sweep rate of applied potential was 25 mV/s at first (from 0 to 25 V). Constant potential of 25 V was then applied. Measured current had three stages: **a** a plunge in the current due to the formation of TiO₂ compact layer, **b** increase in the current because of start of pore formation in the oxide layer and rearrangement of nanotubes in the layer, and **c** constant current towards equalization of the Redox reactions. Panels (●) and (■) represents fluoride ions and [TiF₆]²⁻ complex, respectively

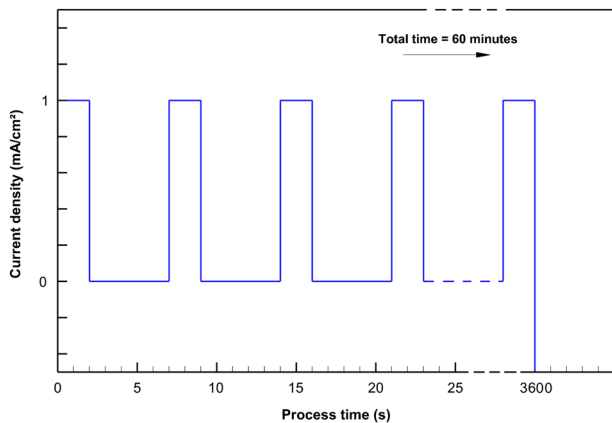
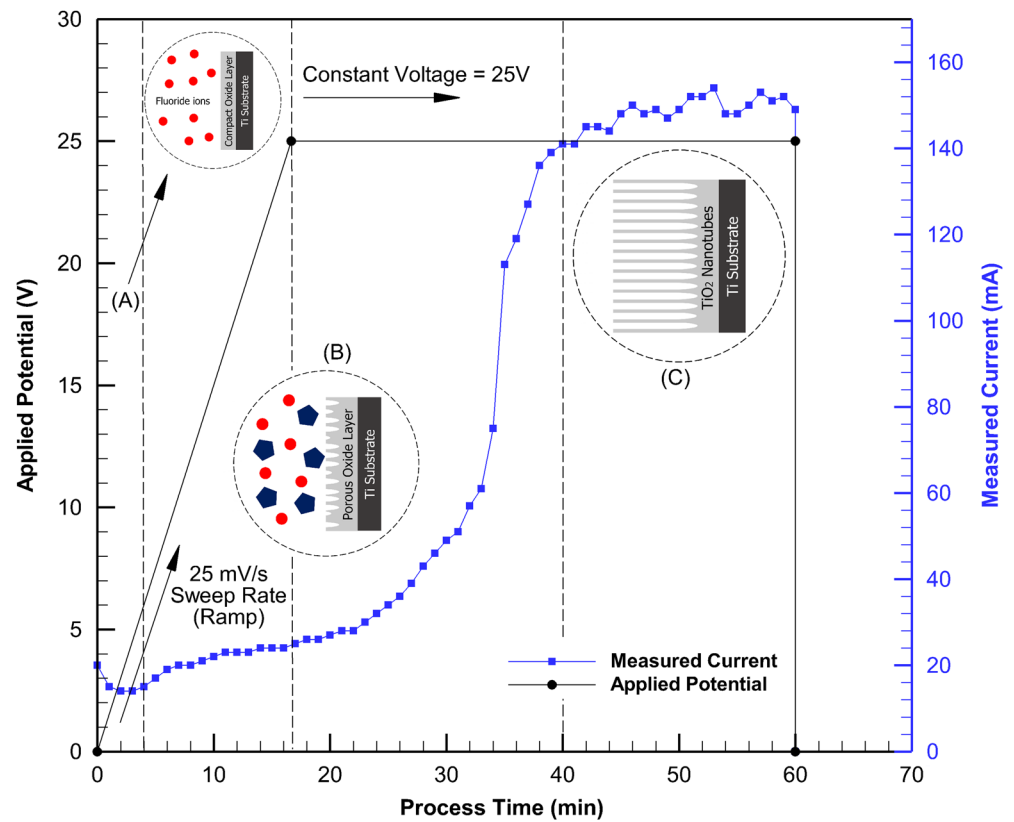


Fig. 2 Schematic representation of pulse current during electro-deposition of HA. Time deposition: $t_{on} = 2$ s, current density: $J_{on} = 1$ mA/cm² and breakdown time: $t_{off} = 5$ s ($J_{off} = 0$ mA/cm²). Total time of the process: 60 min

PAA, Germany) supplemented with 10 % (v/v) fetal bovine serum (FBS, Gibco BRL) and 1 % (v/v) penicillin-streptomycin solution (Gibco), and incubated at 37 °C in a humidified atmosphere containing 5 % CO₂. Medium was replaced every 2 days. When the cells reached 80 % confluence, they were passaged by treatment with 0.05 %

trypsin-EDTA (Gibco), and subsequently counted using trypan blue dye prior to further use.

2.4.2 Cytotoxicity test

The in vitro cytotoxicity of the scaffolds was evaluated by an indirect extract method. Scaffolds were cut into cylindrical samples of 5.5 mm height and 5 mm diameter. The surface area of the samples was ~1.25 cm². Samples were sterilized by exposure to gamma radiation (25 kGy) prior to further incubation at 37 °C in DMEM for 3, 7, and 14 days. The extraction ratio was 1.25 cm² ml⁻¹. Ten samples were extracted for each group of scaffolds. DMEM without scaffolds was also incubated at 37 °C for 3, 7, and 14 days as control. MG-63 cells were seeded in 96-well plate at a density of 10⁴ cells per well 24 h before the end of each extraction period and incubated at 37 °C. After incubation for 24 h, the culture medium was removed and replaced with the extraction media. The plate containing the cells exposed to the extraction media was incubated at 37 °C for 24 h. Subsequently, the extraction media were removed and cell viability was determined by 3-(4,5-dimethylthiazol-2-yl)-2,5-diphenyltetrazolium bromide (MTT) assay.

2.4.3 MTT assay

The MTT assay is based on reduction of yellow tetrazolium salt to purple formazan ((E,Z)-5-(4,5-dimethylthiazol-2-yl)-1,3-diphenylformazan) crystals by dehydrogenase enzymes secreted from the mitochondria of metabolically active cells. According to the standard of ISO 10993-12, after removing the extraction media, 100 μl of MTT solution in DMEM (0.5 mg ml^{-1}) was added into each well and the plate was incubated at 37 °C for 4 h. Subsequently, MTT solution was discarded and the precipitated formazan crystals were dissolved in 150 μl of dimethylsulfoxide. Finally, the optical density (OD) was determined at 545 nm using an Elisa Plate Reader (Molecular Devices, Model Maxline, USA). The intensity of the absorbance is proportional to the number of living cells. This assay was repeated three times and the final ODs normalized to the control OD. The following equations were used to calculate cell viability of the samples:

$$\text{Cytotoxicity \%} = \left(1 - \frac{\text{mean OD of sample}}{\text{mean OD of control}} \right) \times 100 \quad (1)$$

$$\text{Cell viability \%} = 100 - \text{Toxicity \%} \quad (2)$$

2.4.4 Cell morphology

The implants were cut into 10 mm \times 10 mm \times 1 mm sheets. The obtained sheets were sterilized and placed in wells of 48-well plates. Subsequently, 200 μl DMEM supplemented with 10 % FBS was added to each well and the plates were incubated at 37 °C for 12 h (pre-wetting). The medium was then discarded and 2×10^4 of MG-63 cells was seeded into each well and allowed to attach to the samples. The plates were incubated at 37 °C for 24 and 72 h. Subsequently, cellular samples were washed with PBS and then fixed with 2.5 % glutaraldehyde for 12 h. After being rinsed with PBS, samples were dehydrated through a series of graded ethyl alcohols (50, 60, 70, 80, 90, and 96 %) and subsequently air-dried. Finally, samples were sputter-coated with gold and examined under FE-SEM.

2.4.5 Alizarin red staining

The presence of calcium precipitation by MG-63 cells was determined using alizarin red staining. In this experiment, 5×10^3 stem cells were seeded on each sample in a 4-well plate. The cells were kept in osteogenic differentiation culture media (DMEM + F12 + FBS (10 %) + Dexamethasone (10 $^{-7}$ M) + Beta Glycerol phosphate (10 mM) + Ascorbic Acid (50 $\mu\text{g}/\text{ml}$)) for 21 days and incubated at 37 °C in an atmosphere containing 90 % $\text{H}_2\text{O}_{(\text{g})}$ + 5 % CO_2 . During incubation, fresh culture media was added to the

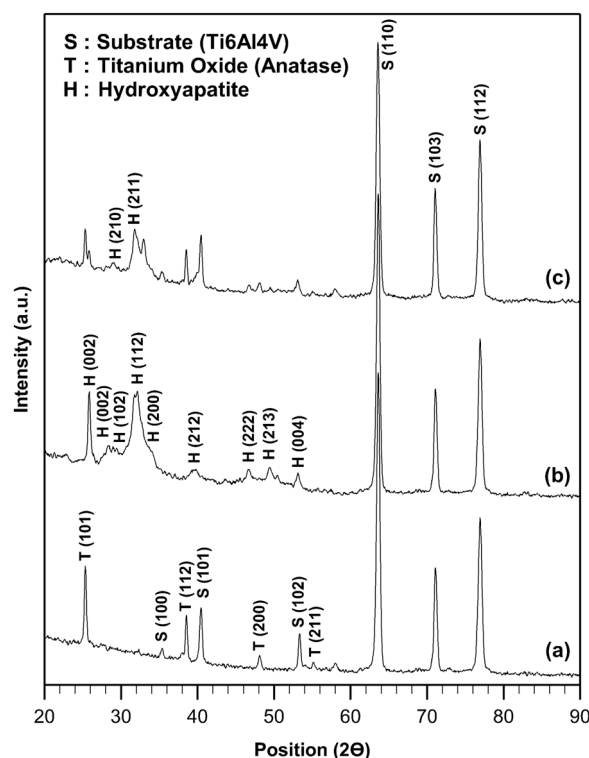


Fig. 3 XRD patterns of **a** anodized layer, **b** HA deposit, and **c** HA/TNTs coating on Ti6Al4V alloy implant. Notice respective intensity shifting of 2000 and 4000 units for clarity of curves (**b**) and (**c**)

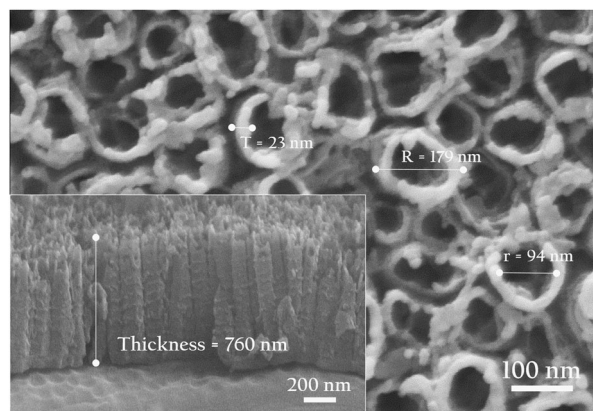
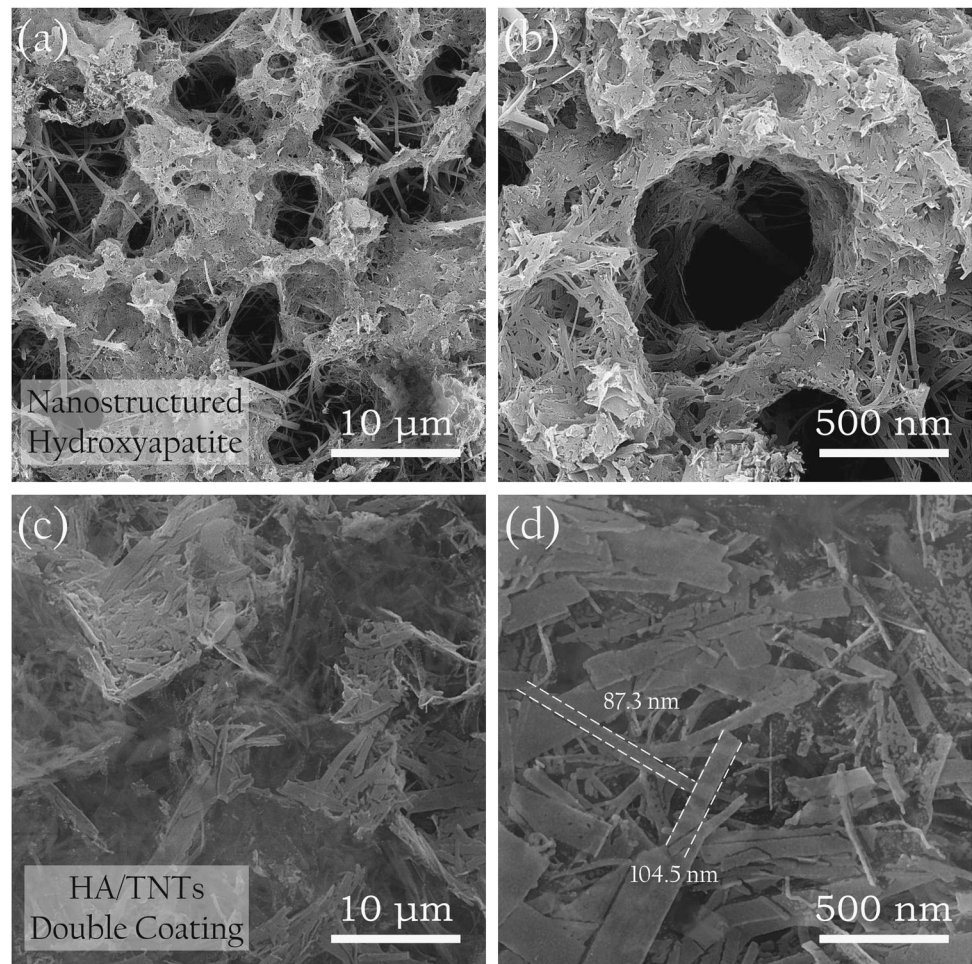


Fig. 4 FE-SEM micrograph of titanium oxide nanotubes synthesized by anodizing process. Layer cross section is shown by the insert picture. Note that mechanical bending was used to separate the nanotubes layer from the substrate

cells every 3–4 days. After that, the culture media was removed and the cellular samples were washed with PBS and fixed with 4 % CH_2O solution for 20–30 min. Subsequently, the cells were washed with PBS solution three times and stained with alizarin red solution (2 %, pH = 5) for 30–45 min at room temperature and dark place. After that, the colored solution was removed and the cells were washed with PBS solution two times and finally, in order to

Fig. 5 FE-SEM images of **a**, **b** pure HA coating and **c**, **d** electrodeposited HA on the anodized Ti6Al4V implant (HA/TNTs)



evaluate and compare calcium mineralization compared to the control, the samples were observed by stereo microscope (Nikon, CSD).

2.5 Surface topography and roughness measurement

Topography and roughness (R_a) of the coated surfaces were studied by atomic force microscopy (AFM, Nanoscope E, Digital Instruments, USA). The indenter tip of the system scanned the surface of the samples. At least five AFM scans were performed on each arbitrary surface. Each value was the average of five measurements.

2.6 Nanomechanical studies

2.6.1 Bonding strength

Bonding strength of deposit with substrate was measured according to ASTM F1044-05 standard. The uniaxial tensile load was applied to the deposit which was bonded to the substrate surface with the epoxy resin using (Model 5565, Instron Co.) at crosshead speed of 10 mm/min. The size of

the samples that used for the bonding strength tests was $30 \times 30 \times 1$ mm. Five measurements were done for each deposit and the mean value was reported to determine the bonding strength.

2.6.2 Nanoindentation and nanoscratch tests

Nanoindentation tests carried out by a TriboScope system (Hysitron Inc. USA), equipped with a Berkovich indenter tip. A triangular Loading-unloading function with a maximum peak load of 70 and 700 μN was applied. In order to the applied load of 70 μN, the peak load was achieved within 5 s and was removed in 5 s without any holding time. For the peak load of 700 μN, the loading-holding-unloading function was 30–10–30 s. Four indentations on each sample applied to achieve reliable results. The nanoscratch tests were carried out by moving the indenter tip while it was in contact with the sample surface at a constant scratching speed of $0.13 \mu\text{m}\cdot\text{s}^{-1}$. The normal load was 700 μN and the length of the scratch was 5 μm. Each sample was scratched three times to achieve reliable results.

Table 1 Nanomechanical properties obtained from bonding strength, nanoindentation and nanoscratch tests

Sample	Elastic modulus (GPa)	Hardness (MPa)	Roughness(nm)	Friction coefficient	Maximum penetration (nm)	Bonding strength (MPa)
Human bone [48, 49]	1.3–25.4	234–760	Nanometric	0.372–0.582	–	–
Polished Ti6Al4V	112 ± 10	4400 ± 400	318	0.42 ± 0.02	–	–
Anodized Ti6Al4V	64.74 ± 4	955.99 ± 10	574	0.32 ± 0.02	286	–
Hydroxyapatite	0.66 ± 0.2	44.35 ± 5	1430	0.65 ± 0.04	>450	12 ± 2
HA/anodized	2.25 ± 0.5	159.27 ± 5	1782	0.46 ± 0.02	352	25.4 ± 2

2.7 Statistical analysis

The statistical calculations were done by the Student's sample *t*-test and values considered significant with less than 5 % of confidence ($p < 0.05$).

3 Results

3.1 Phase analysis, morphology, and microstructure of the coatings

Figure 3 illustrates XRD patterns of the anodized, HA deposit and HA/TNTs double layer coating on the Ti6Al4V alloy implants. As been observed, the oxide layer has been formed of anatase TiO₂ crystal structure. It is interesting to point out that the sharp peaks of TNTs layer releases a dense and concrete nanostructured film. However, appearance of substrate peaks (Fig. 3a) indicated formation of a thin anodized layer. Figure 3b suggests deposition of pure HA on the substrate. No deposition of other calcium phosphates (Octa-calcium phosphates and Tri-calcium phosphates; OCP and TCP) is observed. It should be noted that these compounds (i.e. OCP and TCP) suffer from lower stability, higher dissolving rate, and weaker biological response than pure HA. As is clear from Fig. 3c, diffraction pattern of the HA/TNTs coated samples consists of both HA and anatase phases. It means, the presence of intermediate TNTs layer has no unfavorable effect on synthesis of electrodeposited pure HA coating. However, intensities of some peaks related to the crystal faces of HA layer have been changed with respect to the Fig. 3b. Intensities of the HA peaks related to the HA/TNTs coating, for example, show a decrease compared to the pattern (b) of Fig. 3.

FE-SEM image of titanium oxide layer of anodic nanotubes is illustrated in Fig. 4. The micrograph illustrates a ~760 nm thick porous layer with well-arranged nanotubes. The mean values for nanotubes wall thickness was 23 nm, outside diameter measured 179 nm, and inside diameter was 94 nm. Surface morphologies of pure HA layer and electrodeposited HA coating on the anodized Ti6Al4V alloy implants (HA/TNTs) are shown in Fig. 5. As is observable

in this figure, the nanostructured HA coating consists of both planar and rod-like shapes (Figs. 5a, b). The pure HA layer including considerable porosity with rod-like texture cell walls. It is noteworthy to mention that the deposited HA layer on anodic TNTs presents a uniform and dense morphology, while the same conditions were applied for all electrodeposition procedures. According to Figs. 5c, d, the HA film of the HA/TNTs double layer coating consists of thin small plates which firmly deposited on each other.

3.2 In vitro results

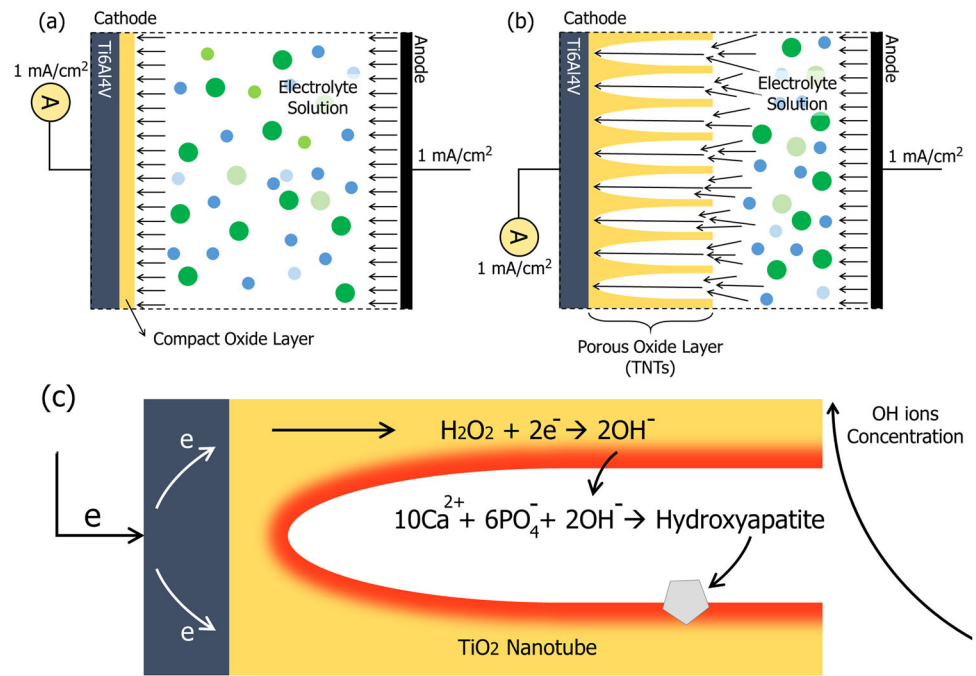
3.2.1 Cytotoxicity study

The in vitro cytotoxicity of samples was measured by MTT assay on osteoblast MG-63 cells. This test determines the mitochondrial activities of vital cells and yields a parameter for their metabolic activities [19]. MG-63 cells were cultured in DMEM in presence of the samples for 1 week. The viable cell percentages of the different samples are given in Fig. 7. Cell viability of the control sample is considered 100 %. Cell viabilities of the extracts of the anodized, HA deposited and HA/TNTs coated implants are 109.27 ± 4.13 %, 91.53 ± 4.65 %, and 94.98 ± 5.53 %, respectively. All these values are higher than that of the uncoated Ti6Al4V sample which indicates 84.63 ± 3.74 %. The increase in cell viability of the scaffolds compared to the bare Ti6Al4V alloy sample was significant ($p < 0.05$) for the coated implants.

3.2.2 Cell attachment and morphology

Figure 8 illustrates the FE-SEM images of the osteoblast cells after 3 h of incubation. As is observable in the Fig. 8, the osteoblast cells have spread over the surface of all specimens. Noticeably, shapes of the cells grown on different specimens are not the same. Spherical cells possessing fewer and shorter filopodia are observed on the polished Ti6Al4V surface as present good biocompatibility but not enough bioactivity of the implant. Conversely, most of the heap osteoblast cells grown on the anodized, HA deposited and HA/TNT coated implants exhibit fine surface anchoring with

Fig. 6 Schematic of the electrochemical setup consisted of a conventional two-electrode configuration for HA deposition on **a** smooth surface of Ti6Al4V cathode and **b** nanotubular TiO₂ coated Ti6Al4V cathode using a constant current density process (1 mA/cm²). **c** Illustrates schematic of a TiO₂ nanotube with high specific surface area. The nanotube platform provides favorable locations for essential reactions and HA formation



long filopodia and spindle-like, polygonal, or widespread shapes which confirms the MTT assay results.

3.2.3 Calcium mineralization and alizarin red staining

Bioactivity of a biomaterial is discussed by means of its ability to regeneration of host living tissue. This property for hard tissue replacements is measured using alizarin red staining test which introduces amount of mineralized calcium on the surface of implant. The calcium mineralization capability is considered as the same grade of bone regeneration value at the implant/bone interface. Alizarin red staining results of polished Ti6Al4V alloy, anodized surface, HA deposited, and HA/TNTs double layer coated prototype implants with control sample have been indicated in Fig. 10. As is clear from Fig. 10a, no calcium has been mineralized on the surface of polished Ti6Al4V alloy implant. It means that the untreated Ti6Al4V surface is not enough bioactive, although showed well biocompatibility due to considerable cell viability and proper cell attachment (Fig. 8a). In other words, uncoated Ti alloy implants consisting of low bioactivity could not promote bone regeneration as results in short-term stabilization of these metallic implants.

3.3 Nanomechanical responses

3.3.1 Topography and surface roughness

Figure 11 compares AFM images of the implant surfaces produced in this research. Mean roughness of our samples

were $0.318 \pm 0.02 \mu\text{m}$, $0.574 \pm 0.06 \mu\text{m}$, $1.429 \pm 0.7 \mu\text{m}$, and $1.782 \pm 0.4 \mu\text{m}$ for polished, anodized, HA deposited, and HA/TNTs coated samples, respectively. The results have been presented in Table 1.

3.3.2 Bonding strength

The bonding strength of the precipitated HA with the Ti6Al4V alloy substrate measured $12.5 \pm 2 \text{ MPa}$. The corresponding value for the HA/TNTs double coating obtained $25.4 \pm 2 \text{ MPa}$. The results of bonding strength tests have been presented in Table 1. This indicated that the presence of TNTs as a middle layer can drastically improve the adhesion strength of HA deposit to the titanium alloy substrate.

3.3.3 Hardness and elastic modulus of surfaces

Nanoindentation tests carried out to study nanomechanical properties of the coated surfaces. Load-displacement curves analyzed to calculate nano-hardness (H) and elastic modulus (E_r) using a power-law fit following the method of Oliver and Pharr [20]. The hardness and elastic modulus of the anodized surface of Ti6Al4V alloy including TNTs were 956 MPa and 65 GPa, respectively, while those of HA coating were approximately measured to be 45 MPa and 0.66 GPa, respectively. The hardness and elastic modulus of HA/TNTs double coating were enhanced to 160 MPa and 2.25 GPa, respectively, when the TNTs were placed as intermediate layer between the HA layer and titanium alloy

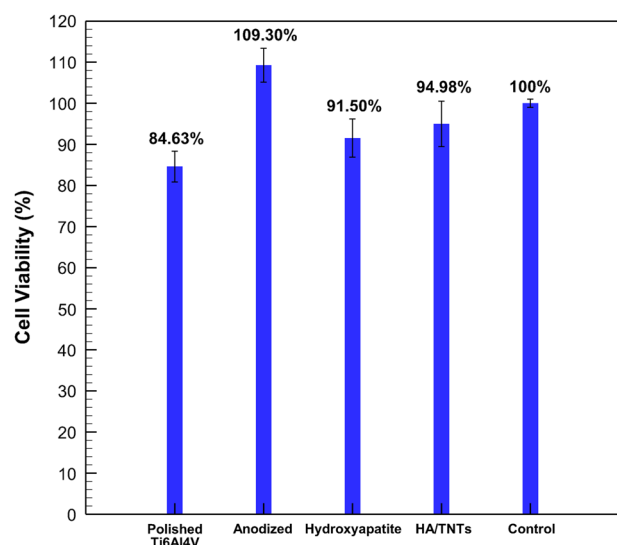


Fig. 7 Cell viability after 1 week of the extracts for: **a** polished, **b** anodized, **c** HA deposit, **d** HA/TNTs coating on Ti6Al4V alloy implant, and **e** control sample. All prototypes exhibit proper viability. The highest biocompatibility belongs to the anodized sample which shows 109.27 % cell viability (indicates significance at $p < 0.05$ in comparison with control)

substrate. The results of nanoindentation measurements on the surfaces have been presented in Table 1.

3.3.4 Nanoscratch results

The representation of scratch test results have been indicated in Figs. 12a–d. Friction coefficient (ξ) is often used to study the nano-scratching properties of materials. This parameter is the ratio of the measured lateral force (F_L) to the exerted normal force (F_N) as:

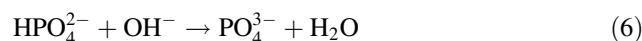
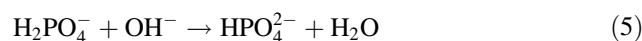
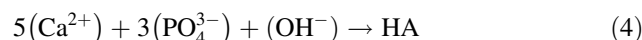
$$\xi = F_L/F_N \quad (3)$$

According to the Fig. 12a, the ξ of the anodized surface was 0.32 ± 0.02 , while the corresponding value of sole HA deposit calculated 0.65 ± 0.04 (Fig. 12b). It is interesting to point out that the ξ of HA layer was enhanced to the 0.46 ± 0.02 in HA/TNTs double coating (Fig. 12c), due to presence of nanotubular TiO_2 intermediate layer.

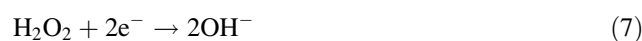
4 Discussion

The XRD analysis revealed that the anodic oxide layer fabricated on Ti alloy implant has been formed of anatase crystal structure (Fig. 3a). Presence of anatase phase in the oxide layer can be due to applied heat treatment at 480°C which leads to phase transformation of the titanium oxide from amorphous to anatase crystals. According to the Eliaz et al. [21], only if pH value of CaP electrolyte is close to 11.6, will the pure HA be precipitated from the electrolyte.

They demonstrated that in presence of enough hydroxyl and phosphate ions in electrolyte, HA phase will be produced through reaction 4. However, according to reactions 5 and 6, production of phosphate ions is also dependent on presence of hydroxyl ions.



This is despite the fact that in all the samples which were coated via the CaP electrodeposition at $\text{pH} = 5.5$, the coating consisted only of the HA phase (Figs. 3b, c). It is noteworthy that the presence of H_2O_2 in the electrolyte and its effect on production of hydroxyl (OH^-) ions should be considered according to the following reaction [22, 23]:



Reaction 7 provides the hydroxyl ions required for reactions 5 and 6. Pure HA is thus synthesized by reaction 4 while enough hydroxyl and phosphate ions are provided by reactions 6 and 7. This decrease could be due to undergo a change of the voltage of precipitation, different ion mobility, high specific surface of cathode which consequently result in difference of speed the probable reactions occurred in the vicinity of the cathode.

According to Fig. 5, the HA deposit formed on anodized sample, present a dense and uniform morphology. However, the pure HA coating precipitated through the same current density, shows a nearly porous structure (Figs. 5a, b). This indicated that the presence of nanotubular titanium oxide as a middle layer can drastically affect evolution of HA formation and subsequently its properties. Based on the similarity of HA electrodeposition processes, the different morphology of HA deposit in HA/TNTs coating can be attributed to the presence of fully porous aligned oxide array which regulates the charge transfer. It means that the TNTs with high specific surface area provide more available places for the essential reactions of HA deposition. The mechanism of HA electrodeposition on the bare Ti6Al4V substrate (with an inherent thin compact oxide layer that proved using EIS measurements by Ahmadi et al. [15]) compared with the anodized Ti6Al4V alloy consisting of TNTs (porous oxide surface) has been presented in Fig. 6.

According to the Fig. 6, during the constant current electrodeposition process, (a) since a smooth surface (polished Ti6Al4V alloy) is placed in the cathode position, the electric current flows uniformly through from all the cathode surface. The mentioned current is which indicated by ammeter. While, (b) when a porous specimen (anodized Ti6Al4V surface including TNTs) is placed as a cathode in

Fig. 8 FE-SEM images of Cell attachment on the **a** uncoated Ti6Al4V alloy, **b** anodized, **c** HA deposit, and **d** HA/TNTs coatings on Ti6Al4V implant

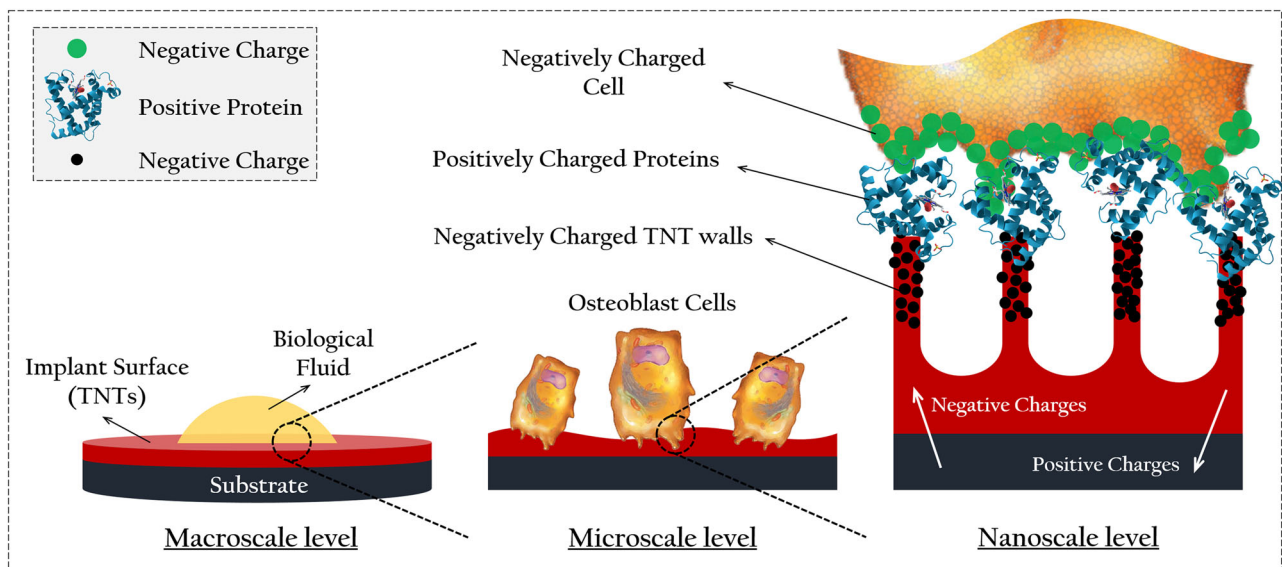
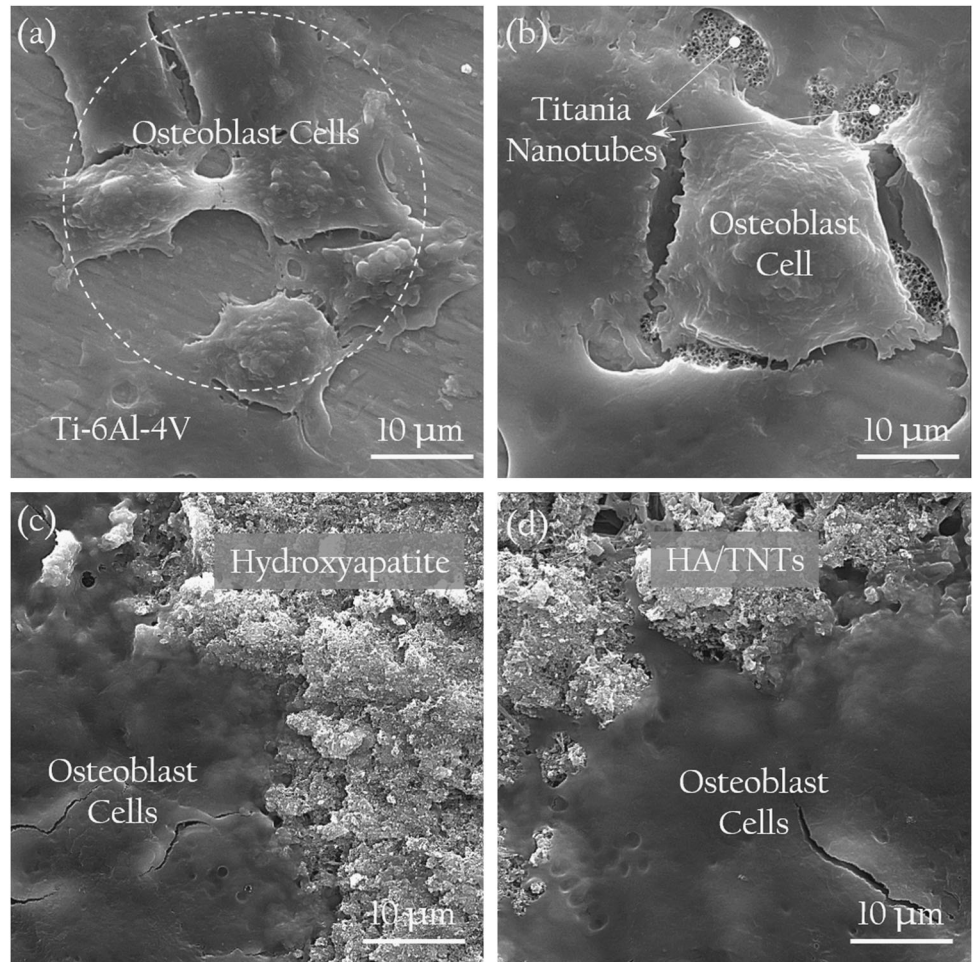


Fig. 9 Mechanism of osteoblast cells attachment onto the nanotubular titanium oxide coating. Proteins with positively charged tips (or positively charged proteins) serve as a bridge (bridging force theory) between negatively charged TiO_2 nanotube walls and negatively charged osteoblast cells.

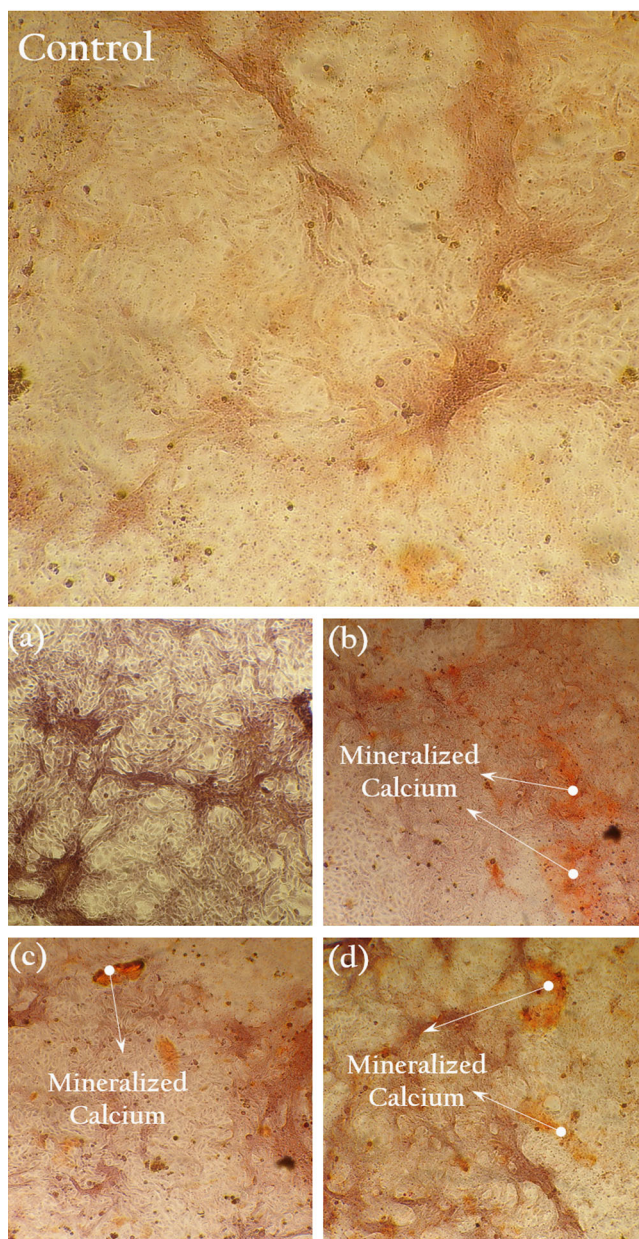


Fig. 10 Images of the alizarin red staining results for: control, **a** polished Ti6Al4V alloy, **b** anodized, **c** HA deposit, and **d** HA/TNTs coated implants. The *red* regions present calcium mineralized on the coated surfaces

the electrolyte solution, the charges and ions could have more opportunities to contribute in the reactions occurring on the surface of nanotubes. Based on the Fig. 6c, the electrons needed for reduction of the H_2O_2 and production of hydroxyl ions (reaction 7), benefit from a high surface area to react. This increasing in value of possible reactions leads to increasing the OH^- ions concentration in the vicinity of the cathode as encourages the HA deposition in association with decrease of the voltage at the interface of cathode/electrolyte in the applied constant current process.

It should be noted that, since the recorded current density by ammeter should be kept constant in the circuit, the charges existing in the electrolyte solution are permitted to move by a lower mobility through the pores of nanotubes in order to compensate the increase of current induced due to many oxidation-reduction reactions on the high specific surface area of oxide layer (anodic TNTs) of the cathode surface. This phenomena is proved according to the following equation:

$$\varepsilon = I_c R \quad (8)$$

where ε is the electric potential, I_c and R are the constant current density and resistance, respectively. Based on fundamental electrical relations, the resistance (R) of anodized porous surface of cathode decreases due to increase the surface area (A -cross sectional area) according to the Eq. 9.

$$R = \rho L/A \quad (9)$$

As ρ is resistivity of the material ($\Omega.m$) and L is length of the element which charges flow along it. As is clear, when the surface area increase, the electrical resistance is reduced as subsequently associated with a voltage decrement in the constant current density process. Therefore, the ions mobility is kept slow and the charges possess enough time to find suitable places for precipitation. Accordingly, a pure, dense, and uniform layer of HA could be deposited on the TNTs platform as confirmed by the FE-SEM micrographs of Figs. 5c, d.

As is clear from Fig. 7, obtained cell viability for the coated prototype implants are in the acceptable biomedical range. Although the high biocompatibility of the HA-based coatings was predicted, the highest cell viability was obtained for the anodized surface consisting of nanotubular titanium oxide. This proper behavior could be attributed to (a) nanostructured surface of anodized layer which is similar to nanosized human tissues, (b) fully porous structure that provides high specific surface, and (c) probable presence of the fluoride ions of electrolyte solution doped into the oxide structure during anodic oxidation process.

Recent studies [24–26] have revealed more desirable properties like good attachment and high proliferation of the fluoride ion-implanted Ti6Al4V alloys than the non-implanted ones. This research proves that TNTs layer is excellent template for cell adhesion and proliferation and can present faster spreading and growth of cells on the anodized implants than the as-polished Ti6Al4V plates. According to Kim et al. [25], the initial cell attachment to titanium oxide layer is much stimulated by F^- ion content. This is in agreement with observations of previous researchers about fluoridated HA coatings [26]. However, they have observed cell proliferation restriction due to Ca^{2+} release reduction in culture medium, when F content of the biomaterial is high.

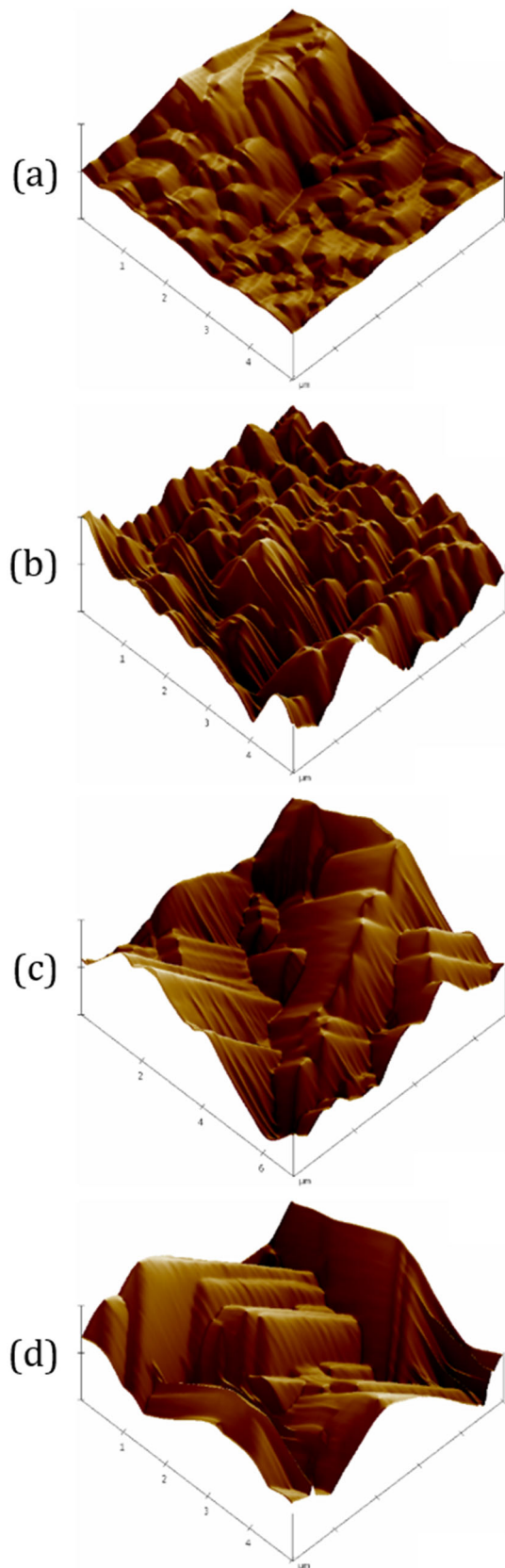


Fig. 11 AFM images of the surface of **a** polished Ti6Al4V alloy, **b** anodized consisting of TNTs, **c** HA deposited, and **d** HA/TNTs coatings on Ti6Al4V implants

The adhesion of osteoblast cells to biomaterials is essential for successful bone/biomaterial interactions. CaP and especially HA-based biological coatings present valuable bioactivity due to provide bone-like template compositionally, as encourage cell attachment and rapid bone regeneration. As is founded from Fig. 8c, d, the appreciate cell anchoring and living tissue interlocking into HA structure promise a long stabilization for these coated implants. While the cell attachment on the anodized surface consisting of TNTs is promoted by different mechanism. The excellent osteoblast cell attachment on the TNTs (Fig. 8b) has been justified by opposite charges attraction theory. Recently, it has been suggested that the surface contact between titanium implant and the membrane of the osteoblast cells consists of two steps: (a) the osteoblast cells membrane makes nonspecific contact due to electrostatic forces [27, 28] and (b) specific binding involving integrin assembly in the focal contact occurs [29–31]. A disputable mechanism for osteoblast cell adhesion to the implant surface has been suggested by previous authors [32, 33]. Based on the hypothesis, the positively charged proteins or proteins with positively charged tips, i.e., a quadrupolar internal charge distribution attached to the negatively charged implant surfaces, serve as a template for the subsequent attachment of the negatively charged osteoblast cells. It has also been shown that a high enough surface charge density on the titanium alloy implant surface and a distinctive internal quadrupolar charge distribution of the protein can change the repulsive force between a negatively charged surface of titanium implant and the osteoblast cells surfaces to an attractive force which is also called the bridging force [27, 28]. The mechanism of cells attachment on the nanotubular TiO₂ layer is presented in Fig. 9.

The origin of the increased binding energy of fibronectin at sharp edges of TNTs oriented vertically may be due to the bridging and direct interaction forces [34, 35]. Accordingly, it has been shown recently that an increase in the negative charges of the titanium surface promotes the fibronectin-mediated binding of osteogenic cell receptors [36]. It should be stressed at this point that the semiconductor anodic titanium oxide nanotube layer is much thicker than the very thin oxide layers formed on flat titanium surface where the bulk titanium properties remain metallic. The surface of the TNTs consist a certain number of titanium and oxygen dangling bonds. Therefore, H⁺ and OH⁻ ions and other ionic species present in the electrolyte can be chemisorbed/adsorbed to the titanium oxide nanotube surface in a curvature-dependent way. Finally, since the nanotubes TiO₂ layer is attached to the underlying metallic titanium substrate, conduction electrons transfer from the titanium alloy substrate to the formed TNTs. In addition, the high porosity and surface area-to-volume ratio of the nanotubular TiO₂ arrays could effectively enhance cellular activity by increasing the efficiency

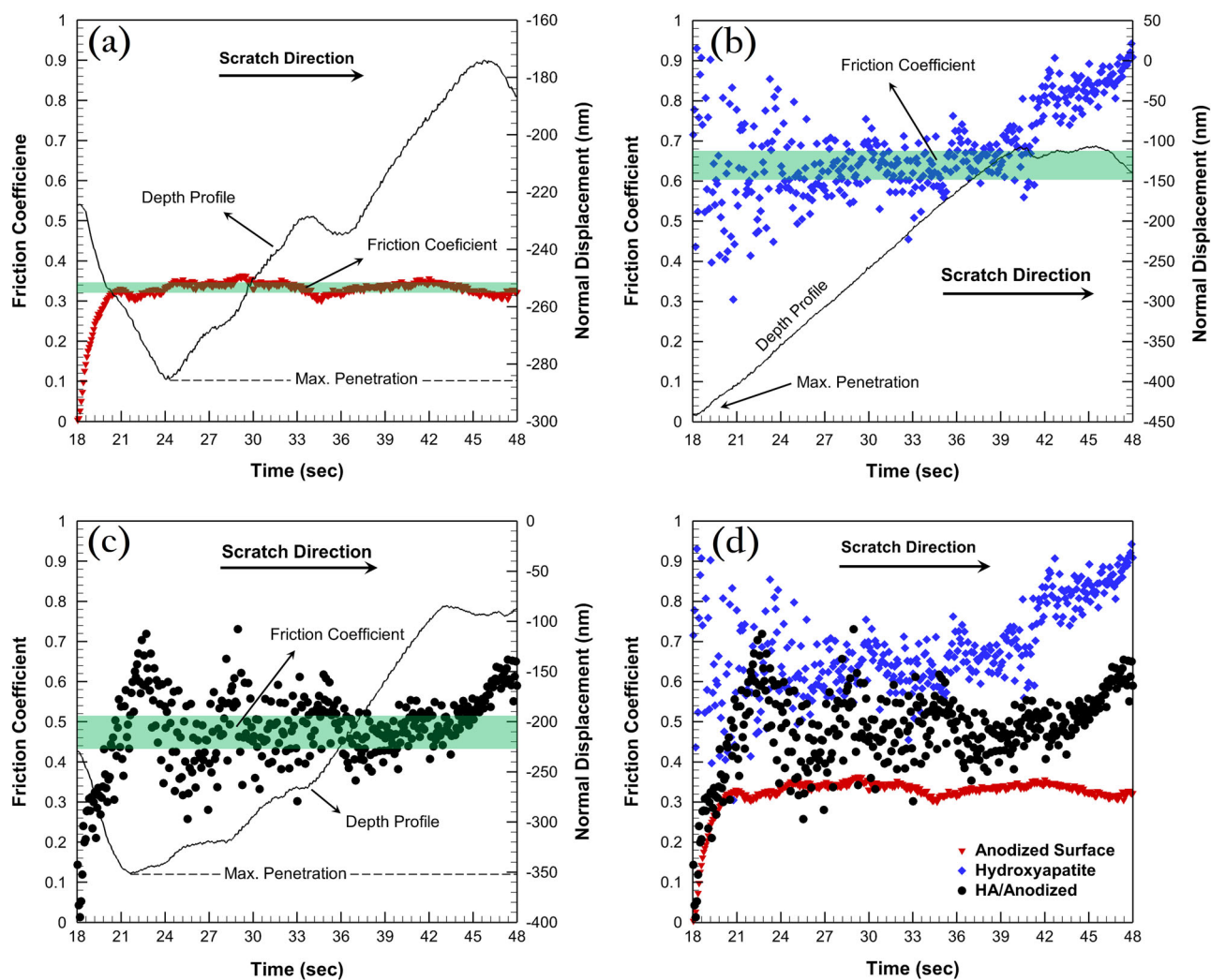


Fig. 12 Nanoscratch results representation of **a** anodized Ti6Al4V surface consisting TiO₂ nanotubes, **b** pure HA deposit and **c** HA/TNTs double layer coatings on Ti6Al4V implant. Highlight regions indicate friction coefficient mean value. Depth profile present normal

displacement of indenter into the surface coating. The comparison show of **d** illustrates a considerable enhancement of ξ obtained for HA layer of HA/TNTs double layer coating compared to the HA deposit due to TNTs intermediate layer

of gas exchange, waste excretion, nutrient delivery, and the transmission of cell signaling molecules [37]. Furthermore, a high surface area provided by the nanostructured coatings suggests useful conditions for interlocking with bone cells and the penetration of body fluid which could properly improve the bone fixation with implant.

The red regions due to the calcium transpiration and the mineralization which are effective factors to bone regeneration, have been encouraged in coated samples (Figs. 10b–d). From a fundamental perspective aimed at understanding the *in vivo* biomineralization process, the growth pathways of improvement the calcium mineralization and apatite formation period at the interface of implant/bone have been the subject of increasing interest over the past decade. It is noteworthy that due to presence of mineral phases and nanosized organics in the human bones, the

bone cells are more interested in nanoscale than microscale environments. In other words, the osteoblast cells can create more calcium on nano surfaces than on micro ones [38]. On the other hand, the existence of Ca and P is also considered as an important factor in mediating osteoblastic cells responses and bone regeneration. It has recently been reported that Ca²⁺ serves as a critical homing signal to recruiting cells for bone regeneration [39]. Meanwhile, inorganic P is known to possess profound effects on bone mineralization, which are mediated by the enzyme ALP [40]. Furthermore, small HA nanoparticles can even penetrate into the cells directly via endocytosis and clathrin coated vesicles to stimulate cell growth [41]. Therefore, the size effects and high surface-to-volume ratio of nanoscale TiO₂ and nanostructured HA-based coatings means that they possess enhanced biological properties over

their microstructure and respective bulk-phase counterparts [42].

Responses of the osteoblast cells to the implants are related to topography, roughness, and composition of the biomaterial surfaces. Morphology of the adherent osteoblasts possesses an important role in regulating the cell behavior [43]. Different topographies resulted in various cell-material interactions. In some cases, high surface roughness leads to improved cell adhesion, proliferation, and ALP activity. Cooper [44] has suggested that increased roughness created by surface modification can affect the formation of bone at the bone/biomaterial interface. In contrary with his observations, although the roughness of anodized surface was lower than the other coated surfaces (Fig. 11 and Table 1), it indicated the best biocompatibility (Fig. 7). This can be attributed to order of magnitude microscale to nanoscale roughness change in HA based and TNTs coated samples.

Presence of large surface area in the anodic nanotubes titanium oxide produced in this research led to biocompatibilities higher than the other samples. Investigations by Webster et al. [45, 46] have suggested greater osteoblast cells adhesion to surfaces with increased nano-roughness. In spite of the difference between microscale and nanoscale rough surfaces, the cell adhesion and proliferation for all of our coated samples were excellent with negligible difference in affinity of the cells. Our results exhibited that the cells cultured onto the rough nanotubes layers spread and extended more filopodia than on smooth layers (Fig. 8). This is because of the presence of the nanotubes which not only exhibit larger surface area, but also provide interlocked cell configuration.

The high measured bonding strength of 25.4 ± 2 MPa for HA/TNTs double layer can thus be attributed to (a) HA-Nanotubes anchoring [15], (b) reinforcement of the cohesive strength of HA with TNTs due to rough surface topography at the HA/TNTs interface, and (c) mechanical interlocking which provides compatible scaffolding [47]. Presence of TNTs as a middle oxide layer in the HA/TNTs double layer coating enhances the interfacial cohesion by superior chemical bonding of titanium oxide with the Ti6Al4V alloy substrate.

Firm adhesion of the coatings to the underlying substrate is of utmost importance for the coatings on implant surfaces. With the purpose to verify the effect of middle TNTs layer on the adhesion strength and scratch behavior of the HA deposit, nanoscratch test was employed.

According to the same deposition procedure and phase of the formed HA precipitation, the improvement of the ξ is corresponded to the porous anodic TiO₂ intermediate layer. Also, according to the depth profiles (Figs. 12a–d), the maximum penetration of indenter into the anodized Ti6Al4V, deposited HA, and HA/TNTs coated surfaces was approximately measured 286 nm, more than 450 nm and

352 nm, respectively, which presents the better mechanical strength of surface coating of HA/TNTs. These nanoscratch behaviors admirably confirmed the obtained results of the adhesion strength and nanoindentation tests.

5 Conclusions

In the present work, the in vitro biological behaviors of polished Ti6Al4V, HA deposited, anodized, and HA/TNTs double layer coated Ti6Al4V alloy were investigated. The measured cell viabilities were 109.27 ± 4.13 %, 91.53 ± 4.65 %, and 94.98 ± 5.53 % for TNTs layer, HA deposit, and HA/TNTs coated samples, respectively. All these figures were higher than 84.63 ± 3.74 % viability of the uncoated Ti6Al4V polished plate. The osteoblast cells were spread over the surface of all the specimens after 3 h of incubation. Different shapes were noticeable on different samples with spherical cells possessing fewer and shorter filopodia on the polished Ti6Al4V plate. Conversely, most of the osteoblast cells were grown on the anodized, HA deposited, and HA/TNTs coated implants. MG-63 cells on the fluoride ion-implanted TNTs coated Ti6Al4V implant showed more efficient behavior, better attachment, and greater proliferation than on non-implanted Ti6Al4V alloy.

The main reason for more efficient biological response of the anodized sample was due to the order of magnitude difference between the nano-sized with the micro-sized HA and HA/TNTs coated surface roughness. The polished, anodized, HA deposited, and HA/TNTs surfaces showed a mean roughness of 0.318 ± 0.02 , 0.574 ± 0.06 , 1.429 ± 0.7 , and 1.782 ± 0.4 μm , respectively.

Nanomechanical responses of the implants were measured using adhesion strength, nanoindentation, and nanoscratch tests. The bonding strength of HA deposit was increased from 12 ± 2 MPa to 25.4 ± 2 MPa using intermediate TNTs layer due to (i) HA-Nanotubes anchoring, (ii) reinforcement of the cohesive strength of HA with TNTs due to rough surface topography at the HA/TNTs interface, and (iii) mechanical interlocking which provides compatible scaffolding. Hardness and elastic modulus of the anodized surface were 956 MPa and 64.7 GPa, respectively. The corresponding values for HA deposit improved from 44.3 MPa and 0.66 GPa to 159.3 MPa and 2.25 GPa for HA/TNTs double layer coating, respectively. Friction coefficient (ξ) of the anodized surface was 0.32 ± 0.02 . The calculated ξ enhanced from 0.65 ± 0.04 for sole HA layer to the 0.46 ± 0.02 for HA/TNTs due to presence of nanotubular TiO₂ intermediate layer.

Compliance with ethical standards

Conflict of interest The authors declare that they have no conflict of interest.

References

- Ahmadi Sh, Sadrnezhaad SK. A novel method for production of foamy core@compact shell Ti6Al4V bone-like composite. *J Alloys Compd*. 2016;656:416–22.
- Elias CN, Lima JHC, Valiev R, Meyers MA. Biomedical applications of titanium and its alloys. *J Miner Metals Mater Soc*. 2008;60:46–9.
- Naddaf Dezfuli S, Sadrnezhaad SK, Shokrgozar MA, Bonakdar S. Fabrication of biocompatible titanium scaffolds using space holder technique. *J Mater Sci: Mater Med*. 2012;23(10):2483–8.
- Ratner BD. A perspective on titanium biocompatibility. In: Brunette DM, Tengvall P, Textor M, Thomsen P, editors. *Titanium in medicine: materials science, surface science, engineering, biological responses and medical applications*. Springer; 2001. pp. 1–10.
- Thomsen MP, Eriksson AS, Olsson R, Bjursten LM, Branemark PI, Ericson LE. Morphological studies on titanium implant inserted in rabbit knee-joints. *Adv Biomater*. 1987;7:87–92.
- Bajgai MP, Parajuli DC, Park SJ, Chu KH, Kang HS, Kim HY. In vitro bioactivity of sol-gel-derived hydroxyapatite particulate nanofiber modified titanium. *J Mater Sci: Mater Med*. 2010;21(2):685–94.
- Hong MH, Lee DH, Kim KM, Lee YK. Improved bonding strength between TiO₂ film and Ti substrate by microarc oxidation. *Surf Interface Anal*. 2010;42(6–7):492–6.
- Oh S, Daraio C, Chen LH, Pisanic TR, Finones RR, Jin S. Significantly accelerated osteoblast cell growth on aligned TiO₂ nanotubes. *J Biomed Mater Res A*. 2006;78(1):97–103.
- Das K, Bose S, Bandyopadhyay A. TiO₂ nanotubes on Ti: influence of nanoscale morphology on bone cell-materials interaction. *J Biomed Mater Res A*. 2009;90(1):225–37.
- Popat KC, Leoni L, Grimes CA, Desai TA. Influence of engineered titania nanotubular surfaces on bone cells. *Biomaterials*. 2007;28(21):3188–97.
- Yang L, Amodio SJ, Barrere-deGroot Fyf, Everts V, Van Blitterswijk CA, Habibovic P. The effects of inorganic additives to calcium phosphate on in vitro behavior of osteoblasts and osteoclasts. *Biomaterials*. 2010;31:2976–89.
- Gopi D, Rajeswari D, Ramya S, Sekar M, Pramod R, Dwivedi J, Kavitha L, Ramaseshan R. Enhanced corrosion resistance of strontium hydroxyapatite coating on electron beam treated surgical grade stainless steel. *Appl Surf Sci*. 2013;286:83–90.
- Mucalo M. *Hydroxyapatite (HAp) for Biomedical Applications, Technology & Engineering*; Woodhead Publishing: Cambridge, UK, 2015.
- Gopi D, Shinyjoy E, Kavitha L. Influence of ionic substitution in improving the biological property of carbon nanotubes reinforced hydroxyapatite composite coating on titanium for orthopedic applications. *Ceram Int*. 2014;41:5454–63.
- Ahmadi Sh, Mohammadi I, Sadrnezhaad SK. Hydroxyapatite based and anodic titania nanotube biocomposite coatings: Fabrication, characterization and electrochemical behavior. *Surf Coat Tech*. 2016;287:67–75.
- Macak JM, Sirotna K, Schmuki P. Self-organized porous titanium oxide prepared in Na₂SO₄/NaF electrolytes. *Electrochim Acta*. 2005;50:3679–84.
- Tighineanu A, Ruff T, Albu SP, Hahn R, Schmuki P. Conductivity of TiO₂ nanotubes: influence of annealing time and temperature. *Chem Phys Lett*. 2010;494:260–3.
- Ghicov A, Tsuchiya H, Macak JM, Schmuki P. Annealing effects on the photoresponse of TiO₂ nanotubes. *Phys Status Solidi A*. 2006;203:R28–30.
- Pariante JL, Kim BS, Atala A. In vitro biocompatibility assessment of naturally derived and synthetic biomaterials using normal human urothelial cells. *J Biomed Mater Res*. 2001;55:33–9.
- Oliver WC, Pharr GM. An improved technique for determining hardness and elastic modulus using load and displacement sensing indentation experiments. *J Mater Res*. 1992;7:1564–83.
- Eliasz N, Sridhar TM. Electrocrystallization of hydroxyapatite and its dependence on solution conditions. *Cryst Growth Des*. 2008;8:3965–77.
- Dreveta R, Benhayounea H, Worthama L, Potirona S, Dougladeb J, Laurent Maquina D. Effects of pulsed current and H₂O₂ amount on the composition of electrodeposited calcium phosphate coatings. *Mater Charact*. 2010;61:786–95.
- Gopi D, Indira J, Kavitha L. A comparative study on the direct and pulsed current electrodeposition of hydroxyapatite coatings on surgical grade stainless steel. *Surf Coat Technol*. 2012;206:2859–69.
- Kung KC, Chen JL, Liu YT, Lee TM. Fabrication and characterization of CaP-coated nanotube arrays. *Mater Chem Phys*. 2014;153:110–16.
- Kim SE, Lim JH, Lee SC, Nam SC, Kang HG, Choi J. Anodically nanostructured titanium oxides for implant applications. *Electrochim Acta*. 2008;53(14):4846–51.
- Cheng K, Weng W, Wang H, Zhang S. In vitro behavior of osteoblast-like cells on fluoridated hydroxyapatite coatings. *Biomaterials*. 2005;26(32):6288–95.
- Abaso D, Gongadze E, Perutková Š, Mateschegewski C, Kralj-Iglič V, Beck U, Iglič A. Mechanics and electrostatics of the interactions between osteoblasts and titanium surface. *Comput Methods Biomec Biomed Eng*. 2011;14(05):469–82.
- Gongadze E, Kabaso D, Bauer S, Slivnik T, Schmuki P, Van Rienen U, Iglič A. Adhesion of osteoblasts to a nanorough titanium implant surface. *Int J Nanomedicine*. 2011;6:1801
- Park J, Bauer S, Von der Mark K, Schmuki P. Nanosize and vitality: TiO₂ nanotube diameter directs cell fate. *Nano letters*. 2007;7(6):1686–91.
- Walboomers XF, Jansen JA. Cell and tissue behavior on micro-grooved surfaces. *Odontology*. 2001;89(1):0002–11.
- Funka WPR. Effects of different titanium alloys and nanosize surface patterning on adhesion, differentiation, and orientation of osteoblast-like cells. *Cells Tissues Organs*. 2005;180:81–95.
- Smeets R, Kolk A, Gerressen M, Driemel O, Maciejewski O, Hermanns-Sachweh B, Stein JM. A new biphasic osteoinductive calcium composite material with a negative Zeta potential for bone augmentation. *Head Face Med*. 2009;5(1):13
- Smith IO, Baumann MJ, McCabe LR. Electrostatic interactions as a predictor for osteoblast attachment to biomaterials. *J Biomed Mater Res A*. 2004;70(3):436–41.
- Zelko J, Iglič A, Kralj-Iglič V, Kumar PS. Effects of counterion size on the attraction between similarly charged surfaces. *J Chem Phys*. 2010;133(20):204901.
- Heath MD, Henderson B, Perkin S. Ion-specific effects on the interaction between fibronectin and negatively charged mica surfaces. *Langmuir*. 2010;26(8):5304–08.
- Xu D, Baburaj K, Peterson CB, Xu Y. Model for the three-dimensional structure of vitronectin: Predictions for the multi-domain protein from threading and docking. *Proteins*. 2001;44(3):312–20.
- Brammer KS, Frandsen CJ, Jin S. TiO₂ nanotubes for bone regeneration. *Trends Biotechnol*. 2012;30(6):315–22.
- Portan DV, Kroustalli AA, Deligianni DD, Papanicolaou GC. On the biocompatibility between TiO₂ nanotubes layer and human osteoblasts. *J Biomed Mater Res A*. 2012;100(10):2546–53.
- Breitwieser GE. Extracellular calcium as an integrator of tissue function. *Int J Biochem Cell Biol*. 2008;40(8):1467–80.
- Suzuki A, Ghayor C, Guicheux J, Magne D, Quillard S, Kakita A, Caverzasio J. Enhanced expression of the inorganic phosphate transporter pit-1 is involved in BMP-2-induced matrix mineralization in osteoblast-like cells. *J Bone Miner Res*. 2006;21(5):674–83.

- 41 Shi Z, Huang X, Cai Y, Tang R, Yang D. Size effect of hydroxyapatite nanoparticles on proliferation and apoptosis of osteoblast-like cells. *Acta Biomater.* 2009;5(1):338–45.
- 42 Zhou H, Lee J. Nanoscale hydroxyapatite particles for bone tissue engineering. *Acta Biomater.* 2011;7(7):2769–81.
- 43 Qu J, Chehroudi B, Brunette DM. The use of micromachined surfaces to investigate the cell behavioural factors essential to osseointegration. *Oral Dis.* 1996;2(1):102–15.
- 44 Cooper LF. A role for surface topography in creating and maintaining bone at titanium endosseous implants. *J Prosthet Dent.* 2000;84(5):522–34.
- 45 Webster TJ, Ejiogor JU. Increased osteoblast adhesion on nanophase metals: Ti, Ti6Al4V, and CoCrMo. *Biomaterials.* 2004; 25(19):4731–39.
- 46 Webster TJ, Schadler LS, Siegel RW, Bizios R. Mechanisms of enhanced osteoblast adhesion on nanophase alumina involve vitronectin. *Tissue Eng.* 2001;7(3):291–301.
- 47 Kodama A, Bauer S, Komatsu A, Asoh H, Ono S, Schmuki P. Bioactivation of titanium surfaces using coatings of TiO₂ nanotubes rapidly pre-loaded with synthetic hydroxyapatite. *Acta Biomater.* 2009;5(6):2322–30.
- 48 Shockey JS, Von Fraunhofer JA, Seligson D. A measurement of the coefficient of static friction of human long bones. *Surf Technol.* 1985;25:167–78.
- 49 Zysset PK, Guo XE, Hoffler CE, Moore KE, Goldstein SA. Elastic modulus and hardness of cortical and trabecular bone lamellae measured by nanoindentation in the human femur. *J Biomech.* 1999;32:1005–12.